Groundwater / Volume 57, Issue 3 / p. 409-419

Research Paper/

Full Access

Conceptualization and Calibration of Anisotropic Alluvial Systems: Pitfalls and Biases

by Guillaume Gianni, John Doherty, Philip Brunner

First published: 03 June 2018
https://doi.org/10.1111/gwat.12802
Citations: 7

Article impact statement: Assuming isotropy or fixed anisotropy may generate biases in the estimation of hydraulic parameters and predictive uncertainty.

Abstract

Physical properties of alluvial environments typically feature a high degree of anisotropy and are characterized by dynamic interactions between the surface and the subsurface. Hydrogeological models are often calibrated under the assumptions of isotropic hydraulic conductivity fields and steady-state conditions. We aim at understanding how these simplifications affect predictions of the water table using physically based models and advanced calibration and uncertainty analysis approaches based on singular value decomposition and Bayesian analysis. Specifically, we present an analysis of the information content provided by steady-state hydraulic data compared to transient data with respect to the estimation of aquifer and riverbed hydraulic properties. We show that assuming isotropy or fixed anisotropy may generate biases both in the estimation of aquifer and riverbed parameters as well as in the predictive uncertainty of the water table. We further demonstrate that the information content provided by steady-state hydraulic heads is insufficient to jointly estimate the aquifer anisotropy together with the aquifer and riverbed hydraulic conductivities and that transient data can help to reduce the predictive uncertainty to a greater extent. The outcomes of the synthetic analysis are applied to the calibration of a dynamic and anisotropic alluvial aquifer in Switzerland (The Rhône River). The results of the synthetic

and real world modeling and calibration exercises documented herein provide insight on future data acquisition as well as modeling and calibration strategies for these environments. They also provide an incentive for evaluation and estimation of commonly made simplifying assumptions in order to prevent underestimation of the predictive uncertainty.

Introduction

In the context of simulating surface-water groundwater interactions, the aquifer and riverbed properties are often estimated (Lavigne et al. 2010; Maheswaran et al. 2016; Brunner et al. 2017; Yihdego et al. 2017; Zhou et al. 2018). In current modeling practice, models tend to be calibrated using observations of hydraulic heads under the assumption of horizontally isotropic hydraulic conductivity fields. However, alluvial aquifers are formed by successive vertical and horizontal overlays of channel-bar and channel-fill deposits (Bridge and Demicco 2008). At a broad scale, the continuity of these geological formations which present different hydraulic properties can lead to a high degree of anisotropy (Kenoyer 1988; Zlotnik et al. 2011; Jha et al. 2016), reaching values as high as 20 (Kruseman and de Ridder 1994). For shallow alluvial aquifers, the horizontal anisotropy plays an important role in controlling the water table throughout the aquifer (Quiñones-Aponte 1989; Cihan et al. 2014). The impact of horizontal anisotropy on flow through aquifers has mainly been studied for the recovery of hydrocarbons, CO_2 sequestration, and in geothermics. Willems et al. (2017), for example, showed that an incorrect assumption of isotropic conditions can lead to significant underestimation of geological risks associated with geothermal doublets.

Numerous methods based on aquifer tests have been developed to estimate the horizontal aquifer anisotropy (Kucuk and Brigham 1981; Neuman et al. 1984; Mutch 2005; Mathias and Butler 2007). Recently, innovative methodologies based on geophysical measurements (electrical anisotropy, values of microgravity) have been developed (Al-Hazaimay et al. 2016; Fernandez-Alvarez et al. 2016), but are still not widely used. Therefore, information on the degree of horizontal anisotropy of an aquifer may not be available. Furthermore, estimation of its value may be omitted from the model calibration process, with isotropy assumed for convenience. In some cases, the need for estimating anisotropy may arise through an inability to achieve a satisfactory fit with observed heads, thereby obviating a structural component of misfit born of an erroneous assumption of isotropic condition. However, in other (probably more common) circumstances, an isotropic assumption may not compromise the attainment of a satisfying fit with the calibration dataset, despite the fact that anisotropic conditions may indeed prevail. Under these circumstances, estimates of hydraulic conductivity may incur bias as this parameter adopts a surrogate role to compromise for the erroneous assumption of isotropy. This, in turn, may engender bias in model predictions, which are sensitive to the horizontal anisotropy of the aquifer hydraulic conductivity. Additionally, the influence of the river on local groundwater dynamics may be significant and is often dominated by riverbed hydraulic properties (Winter et al. 1998; Fleckenstein et al. 2010; Gianni et al. 2016; Partington et al. 2017; Tang et al. 2017). It follows that the estimation of the riverbed hydraulic conductivity should be included in the calibration process and that the uncertainty of its estimation should feature in model-based predictive uncertainty analysis.

The above discussion suggests the following set of questions:

1. To what extent can a false assumption of horizontal isotropy of an alluvial aquifer influence the model predictions and associated uncertainties?
2. Are steady-state hydraulic head observations sufficient to estimate the riverbed and aquifer hydraulic

properties, including the horizontal anisotropy of the aquifer? What are the implications for predictive uncertainty?

3. Can transient observations of hydraulic heads further constrain the estimation of parameters than steady-state observations?

The goal of this paper is to analyze these questions using numerical models and state-of-the-art calibration approaches. First, the underlying theory of the employed calibration and uncertainty analysis is briefly described. Then, the biases in estimated parameters and predictive uncertainty are explored through synthetic modeling. The information content of head observations is subsequently quantified for steady-state and transient conditions. Finally, based on the insights gained from the synthetic analysis, the calibration of a model simulating the interaction between the Rhône River in the area of Sion (Switzerland) and its alluvial aquifer is performed.

Methods

In this section, we present formal methods through which the well- or ill-posedness of an inverse problem, as well as its consequences in terms of predictive uncertainty, can be quantified (Doherty 2015).

Truncated Singular Value Decomposition

A matrix Z has a "null space" if there exists a non-zero vector x for which

$$0 = Zx. \tag{1}$$

In the present context, we suppose that the matrix Z represents the action of a model on its parameters x to produce a set of outputs employed for model calibration. If Equation 1 holds, then a null space exists. Consequently, if a parameter set can be found that fits the calibration dataset, it is possible to find another set of parameters that also fits to the same extent the calibration dataset, simply through addition of x to the parameter set. Non-uniqueness and the existence of a null space are thus two descriptions of the same phenomenon. The non-uniqueness, also referred to herein as "parameter correlation" or "postcalibration correlation," results from an insufficiency of information provided by the calibration dataset with respect to that required for unique resolution of the correlated parameters.

The sensitivity matrix J of model outputs to estimated parameters (often referred to as the Jacobian matrix) is used to represent the linearized action of the model on its parameters under calibration conditions. It can be used in place of Z and thus singular value decomposition can be employed to regularize ill-posed inverse problems. Singular value decomposition of the sensitivity matrix J gives

$$J = USV^t, \tag{2}$$

where U is an orthonormal matrix whose columns span model "output space," V^t is the transpose of V, another orthonormal matrix. The columns of span the "parameter space." is a matrix whose diagonal

V S

elements contain singular values. These values are arranged from highest to lowest starting from the top and ranging to zero. The number of singular values, which are significantly different from zero, defines the number of dimensions of the "solution space." According to where singular values approach zero, the V matrix can then be partitioned as (Moore and Doherty 2005)

$$V = [V_1 V_2].$$

(3)

This outcome is also referred as "truncated singular value decomposition." When partitioned in this way, the columns of V_1 span the solution space while those of V_2 span the null space. The columns of V_1 define combinations of parameters which are uniquely estimable on the basis of the calibration dataset, while the columns of V_2 identify combinations of parameters which belong to the null space, and are hence inestimable.

Parameter Identifiability and Predictive Uncertainty

The "identifiability" of a parameter quantifies the ability of the calibration process to uniquely resolve its value. Doherty and Hunt (2009) show that this statistic can be viewed in two ways. First, it is the square of the cosine between a parameter and the projection of that parameter into the solution space. It is also the diagonal element of the "resolution matrix" as it pertains to that parameter. The resolution matrix R expresses the relationship between the estimated value of a parameter and the true, but unknown, value of that parameter. Where regularization is achieved through singular value decomposition, the resolution matrix is an orthogonal projection operator onto the calibration solution space expressed as

$$R = V_1 V_1^t.$$

(4)

If an inverse problem is well-posed, the resolution matrix is the identity matrix. If it is ill-posed, the diagonal elements pertaining to at least some parameters will be less than 1, they may be as low as zero. The identifiability of a parameter is thus a number that can range between 0 and 1. If it is 0, the calibration dataset carries no information with respect to that parameter. If it is 1, the parameter can be estimated uniquely, but not without error because of the presence of measurement noise in the calibration dataset. Where the identifiability of a parameter is smaller than 1, the calibration dataset contains information with respect to this parameter, but insufficient information to support its unique estimation. This is an outcome of the sharing of calibration information with other parameters. The parameter thus suffers postcalibration correlation with one or more of the other parameters. The identities of these other parameters, and the extent of their correlations, may be ascertained through inspection of the columns of the matrix V_1. An alternative means of specifying this correlation is to examine the posterior parameter covariance matrix calculated using the linearized form of Bayes equation as (Doherty 2015)

$$C_{\text{post}(k)} = C_{\text{pre}(k)} - C_{\text{pre}(k)} J^t \left[J C_{\text{pre}(k)} J^t + C_{(\varepsilon)} \right]^{-1} J C_{\text{pre}(k)},$$

(5)

where $C_{\text{pre}(k)}$ is the prior covariance matrix of parameters that are estimated through the calibration process while $C_{(\epsilon)}$ is the covariance matrix of measurement noise.
Considering a prediction s of management interest made by a model and the sensitivity vector y_s of this prediction with respect to model parameters. The pre- and postcalibration variance of predictive uncertainty can be calculated from the prior and posterior parameter covariance matrices, respectively,

$$\sigma^2_{\text{pre}(s)} = y_s^t C_{\text{pre}(k)} y_s,$$

(6)

$$\sigma^2_{\text{post}(s)} = y_s^t C_{\text{post}(k)} y_s.$$

(7)

The reduction in the predictive uncertainty variance, achieved between $\sigma^2_{\text{pre}(s)}$ and $\sigma^2_{\text{post}(s)}$, is dependent on the conditioning provided by the calibration dataset.

In the following section, synthetic observation data using a steady-state, anisotropic model are generated and then used to estimate hydraulic parameters in a model where horizontal isotropy is falsely assumed.

Synthetic Modeling

Model Design

A synthetic model of a river-aquifer system was developed to analyze the questions raised in the introduction. The conceptual model consisted of a losing river flowing across a shallow, silty-gravely, horizontally anisotropic alluvial aquifer surrounded by impermeable geological formations (Figure 1A).

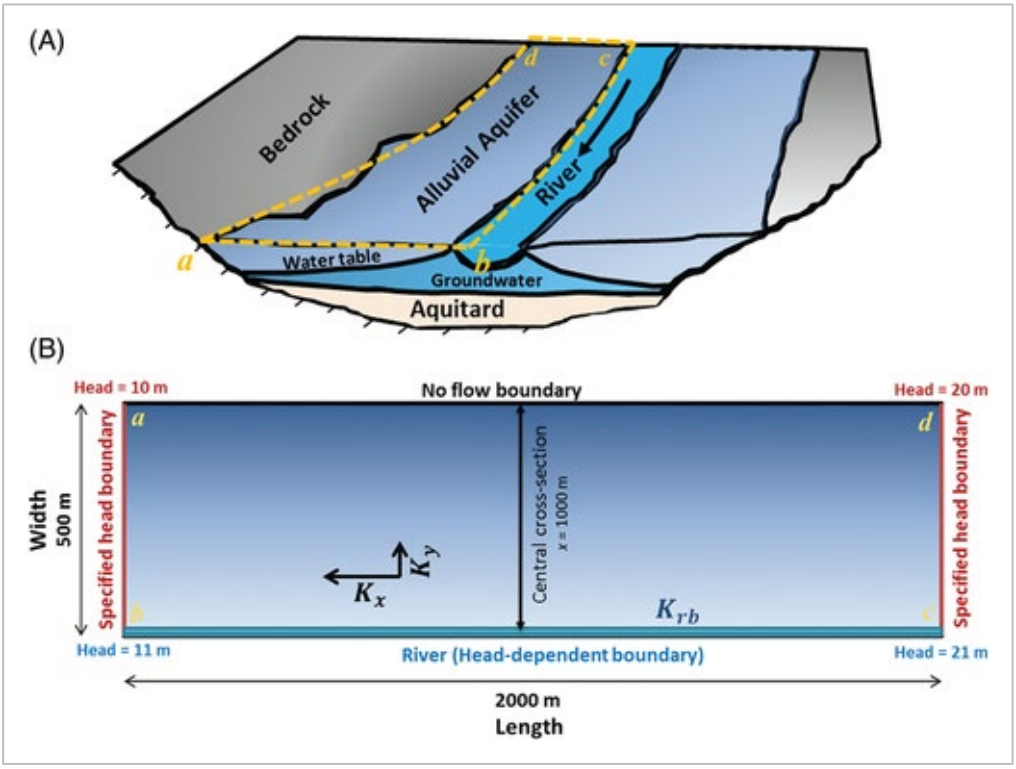

Figure 1

Open in figure viewer | PowerPoint

(A) Conceptual model of an alluvial aquifer traversed by a losing river (flowing from *c* to *b*) and surrounded by an impermeable bedrock and an aquitard. (B) Numerical model design and boundary conditions based on the conceptual model.

The dimensions of the model domain were 2 km in the longitudinal direction and 500 m in the transverse direction. The water table had a regional gradient, equal to the river slope, of 0.5%. Specified heads along the right edge (line *cd*) and left edge (line *ab*) of the model domain were 20 and 10 m, respectively. The aquifer bottom elevation increased linearly from 0 to 10 m from *ab* to *cd*. Along the lower edge of the model domain (line *bc*), a head-dependent boundary representing the river was imposed. The head values decreased linearly from 21 to 11 m from *c* to *b*, for steady-state simulations. For transient simulations, the entire head-dependent boundary (river stage) was uniformly varied.

Aquifer parameters were the hydraulic conductivity parallel to the river K_x [L/T] (direction of maximum hydraulic conductivity) and the hydraulic conductivity perpendicular to the river K_y [L/T] (direction of minimum hydraulic conductivity). The horizontal anisotropy of the aquifer A_h was defined as the ratio K_y/K_x [-]. The riverbed hydraulic properties were represented by the conductance K_{rb} [L/T]. The specific yield of the aquifer S_y [-] was set to a value of 0.2 (Morris and Johnson 1967).

The head distribution over the model domain was obtained using the finite-element modeling package FEFLOW 7.0, developed by DHI-WASY, (Diersch 2014), which solves the flow equation for two-dimensional horizontal flow in an unconfined anisotropic aquifer

$$\frac{\partial}{\partial x}\left(K_x h \frac{\partial h}{\partial x}\right) + \frac{\partial}{\partial y}\left(K_y h \frac{\partial h}{\partial y}\right) = S_y \frac{\partial h}{\partial t}, \quad (8)$$

where h [L] is the hydraulic head and t [T] is the time. Head observations are monitored along the *central cross section* (Figure 1B).

Bias in Estimated Parameters

The water table elevations along the *central cross section* of the synthetic anisotropic model were calculated using parameter values of $K_x = 10^{-3}$ m/s, $K_{rb} = 10^{-4}$ m/s, and $A_h = 0.1$. These observed heads are subsequently used as calibration targets in order to estimate the hydraulic parameters and the predictive uncertainties. Different geometric configurations of observation wells along the *central cross section* were used as calibration targets for the same model but isotropic ($A_h = 1$), in steady-state condition, where the parameters K_x and K_{rb} were estimated. K_y was therefore equal to the value of K_x. An objective function, representing the average discrepancies between simulated and observed heads, was calculated.

For each calibration instance, a set of two head observations, extracted along the *central cross section*, was selected to establish the calibration dataset. A total of 120 well pairs were used. Each pair was defined through two identifying variables: the distance of the well closest to the river (symbols in Figure 2A and 2B) and the distance between the two wells (see x-axis in Figure 2A). For each calibration exercise, the model-to-measurement misfit was minimized (see y-axis in Figure 2A). No measurement noise was added to the head measurements. Hence, failure to achieve an objective function of zero was the outcome of structural noise incurred by the wrong assumption of horizontal isotropy that was employed when calibrating the model. By calibrating the model against the different spatial configurations of the synthetic head observations along the *central cross section* (Figure 1B), the implications of the false assumption of isotropy could be established.

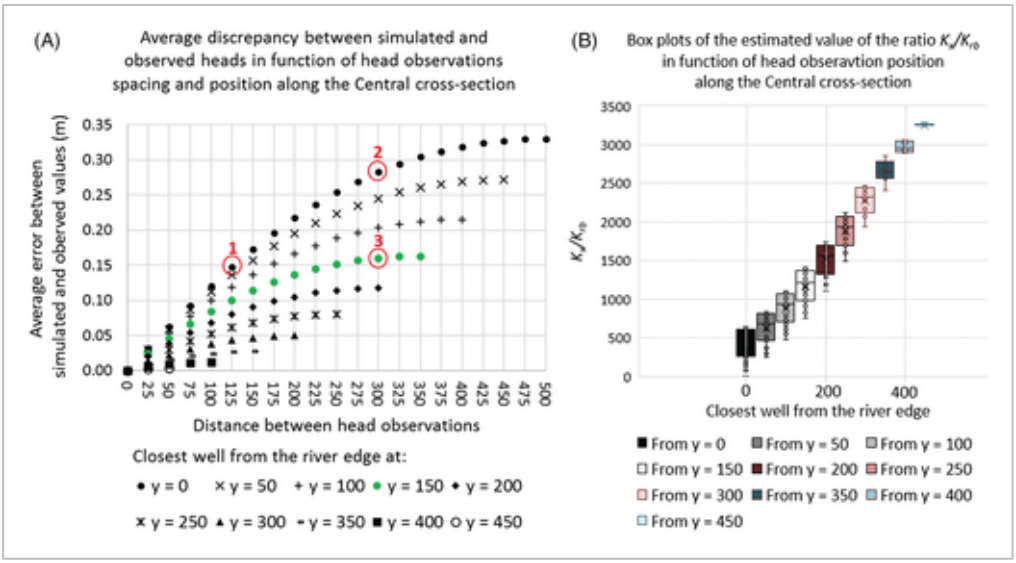

Figure 2

Open in figure viewer | PowerPoint

(A) Postcalibration average error between simulated ($A_h = 1$) and observed ($A_h = 0.1$) heads plotted against the distance between head observations for different values of the distance of the closest well to the river. (B) Box plots of the estimated ratio K_x/K_{rb} (the actual value is 10). Each box plot summarizes the results for different distances between two head observations and a fixed distance of the closest well to the river edge.

Figure 2A depicts the final average error between observed head values and their computed counterparts

plotted against the distance between the wells of each well pair. For instance, point 1 shows the postcalibration average error with the closest well to the river located at the river edge ($y = 0$) and the second well at a distance of 125 m. Point 2 represents the average error with the same first well ($y = 0$) and a more distant well at 300 m. In both cases, the closest well to the river is the same, only the distance separating the two wells in each pair changes. The larger distance separating the two wells causes the average misfit to be higher for point 2. The same remark can be made for other well pairs. For points 2 and 3, the distances separating the two wells in these cases are the same (300 m). However, the average misfit is higher for point 2 than for point 3. The smaller distance of the closest well to the river caused the average misfit to be higher for point 2 ($y = 0$) than for point 3 ($y = 150$). The same remark can be made for other well pairs. Therefore, it is clear that not only the distance between the wells influences the value of the postcalibration misfit, but also the distance between the river and its closest well. Furthermore, although a post-calibration misfit was systematically present when two distinct observation wells were used as calibration targets, for many configurations the error between observed and simulated values is very small. Therefore, considering real world datasets, certain values of the postcalibration average error may be commensurate with the one expected according to measurement error that would prevail in real world datasets. Consequently, many of the fits depicted in Figure 2A could thus be construed as "good" or "satisfying" fits.

Concerning the estimation of the parameters representing the hydraulic properties of the aquifer and the riverbed, that is, K_x and K_{rb}, their estimated ratio K_x/K_{rb} achieved through the calibrations are shown in Figure 2B. The value of this ratio is of particular importance for surface water groundwater interactions as it is the key parameter in the Boussinesq equation that determines the shape of the water table profile perpendicular to the river (Brunner et al. 2009). The box plots represent the range of values estimated for K_x/K_{rb} for groups of well pairs (the actual value is 10). A systematic overestimation of this ratio results from the false assumption of horizontal isotropy. Overestimations by more than two orders of magnitude occur for most of the observation well configurations ($y = 150$ to $y = 450$).

These results illustrate that although in some cases the incorrect assumption of isotropic conditions can be revealed by a compromised fit with the calibration dataset, in other cases an acceptable fit with the dataset can be achieved (i.e., a fit that is commensurate with that expected from measurement noise). Moreover, a wrong assumption of horizontal isotropy might lead to significant errors in the estimation of key parameters, such as K_x to K_{rb}. The next section assesses the consequences on the estimation of predictive uncertainty.

Errors in Quantification of Predictive Uncertainty

The precalibration and postcalibration uncertainty of the predictions of the water table at distances of 10, 20, 40, 100, 200, and 400 m from the river along the *central cross section* were calculated. In each case, a steady-state head observation at one of the aforementioned distances was used as calibration target and the uncertainty of the predictions at the remaining distances from the river were calculated.

The pre- and postcalibration predictive uncertainties were calculated using Equations 6 and 7, respectively. In each case, the predictive uncertainties were calculated for two different calibration setups: (1) The horizontal anisotropy was assumed to be known and then only K_x and K_{rb} were estimated and (2) all the three parameters K_x, K_{rb}, and A_h were estimated. For the purpose of synthetic analysis, arbitrary but sensible matrices $C_{(\epsilon)}$ and $C_{\mathrm{pre}(k)}$ were defined, following the description in Doherty (2015). $C_{(\epsilon)}$ was assumed to be diagonal with elements equal to 0.01 m^2. $C_{\mathrm{pre}(k)}$ was also assumed to be diagonal, with all diagonal elements equal to 1.0 for K_x and K_{rb}, and 0.5 for A_h (the values pertain to the logs to base 10 of the estimated parameters).

Figure 3 shows the estimates of the pre- and post-calibration predictive uncertainties. The squares represent the precalibration (red) and postcalibration (green) predictive uncertainties calculated through the calibration of only K_x and K_{rb}. The triangles represent the precalibration (red) and postcalibration (green) predictive uncertainties calculated through the calibration of K_x, K_{rb}, and A_h. For all cases that admit no prior uncertainty on A_h, predictive uncertainties associated with the water table elevation are systematically underestimated. This underestimation follows from the false assumption of perfect knowledge of A_h. If prior uncertainty in A_h is admitted, the magnitude of the predictive uncertainty is significantly influenced by the location of both the calibration targets and the predictions. For example, high uncertainty remains if the calibration targets are close to the river and the water table predictions are far from it (Figure 3, top row).

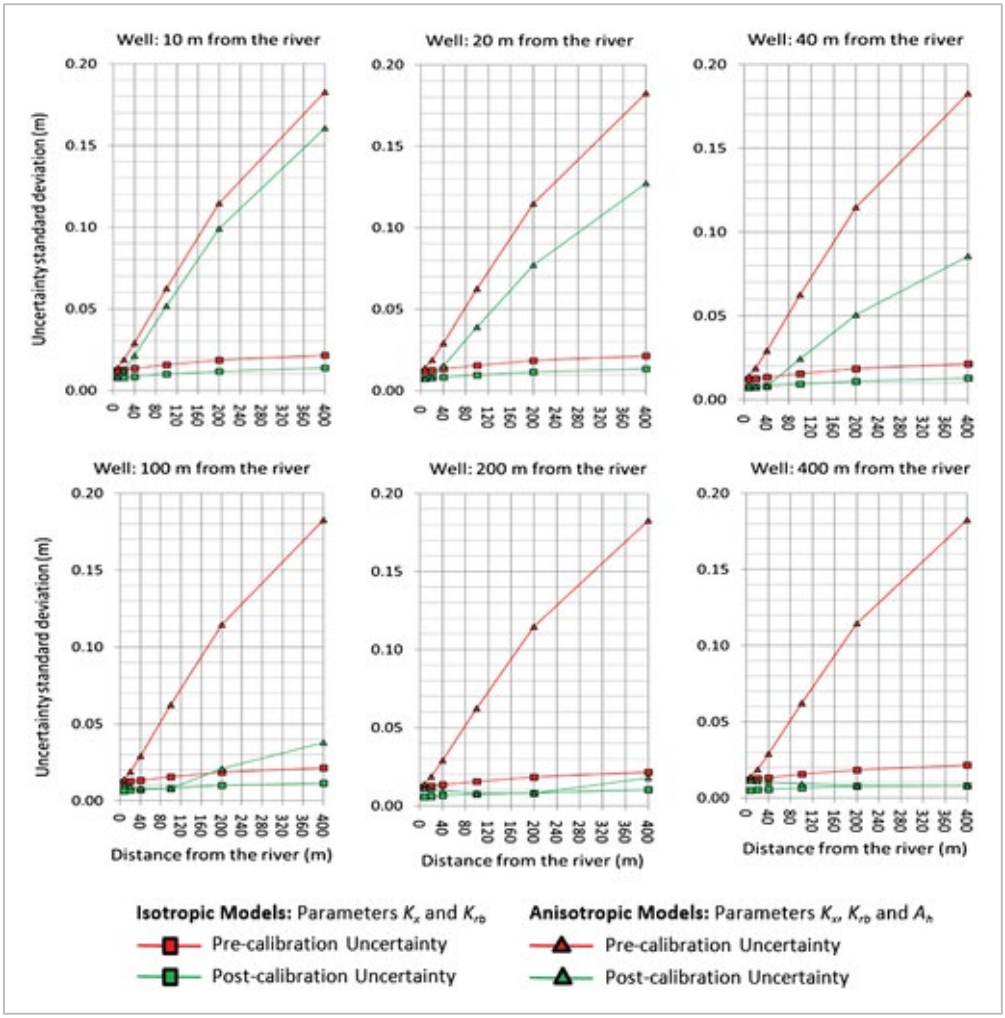

Figure 3

Open in figure viewer | PowerPoint

Estimation of the pre- and postcalibration predictive uncertainties for calibrations including solely K_x and K_{rb} (assuming knowledge of A_h) and including all parameters K_x, K_{rb}, and A_h at different distances from the river (10, 20, 40, 100, 200, and 400 m). The title of each graph designates the distance from the river of the calibration target.

This analysis illustrates the importance of including aquifer horizontal anisotropy as an adjustable parameter in the uncertainty analysis process. Failure to include it as an adjustable parameter in the calibration process may result in unquantifiable parameter and predictive biases. Although inclusion of A_h in the calibration process may not result in a unique estimation of its value, it does reduce errors in the calculation of predictive uncertainty. Conversely, omitting the horizontal anisotropy from the calibration can cause an underestimation

of the uncertainty in the water table predictions. The extent to which observations of hydraulic heads for both steady-state and transient calibrations can inform the parameters, when jointly estimated, and thus reduce the postcalibration predictive uncertainty, is discussed in the next sections.

Parameter Identifiability for Steady-State and Transient Calibrations

The identifiability of the parameters K_x, K_{rb}, and A_h, and thus the potential reduction of their uncertainties and those of predictions that are sensitive to these parameters, was analyzed by calculating the resolution matrix R using Equation 4. The identifiability of each parameter, according to the calibration approach, is equal to the respective diagonal element of the resolution matrix associated with that calibration approach (Table 1A to D).

Table 1. Results of the parameter identifiability analysis

	S				R			V_1		
A	0.50	—	—	K_x	**0.04**	0.04	0.12	0.20	—	—
	—	—	—	K_{rb}	*	**0.04**	0.12	0.19	—	—
	—	—	—	A_h	*	*	**0.37**	0.61	—	—
B	0.57	—	—	K_x	**0.50**	0.50	0.00	0.00	0.71	—
	—	0.10	—	K_{rb}	*	**0.49**	0.00	0.00	0.70	—
	—	—	—	A_h	*	*	**1.00**	1.00	0.00	—
C	2.00	—	—	K_x	**0.19**	0.00	0.49	−0.31	−0.63	—
	—	0.10	—	K_{rb}	*	**1.00**	0.00	0.90	−0.44	—
	—	—	—	A_h	*	*	**0.49**	−0.31	−0.63	—
D	0.60	—	—	K_x	**1.00**	0.00	0.00	0.02	−0.23	−0.97
	—	0.07	—	K_{rb}	*	**1.00**	0.00	−0.02	0.97	−0.23
	—	—	—	A_h	*	*	**1.00**	1.00	0.01	0.01

The parameter names are displayed next to associated elements for the Matrix R (the Resolution Matrix, for which values along its dia represent the identifiability of each parameter) and V_1 (combinations of parameters, which are uniquely estimable). S is the matrix of singular values. Symmetric values are replaced by the symbol (*) and null values are replaced by the symbol (—) for better readability. Results of the parameter identifiability analysis using (A) one well; (B) two wells, note that through adding more observation wells the results are nearly identical (results not shown); (C) one transient observation well located 10 m away from the river—the model is calibrated against head difference targets; (D) two transient observation wells located 10 and 400 m away from the river—the model is calibrated against head value targets, not the differences.

First, the calibration dataset was provided with one observation along the *central cross section*. The results

are shown in Table 1A. The dimensionality of the solution space is one (only one observation). The identifiability of A_h is significantly smaller than 1, while those of K_x and K_{rb} are close to 0. Similar results were obtained for observation wells located at different positions along the *central cross section* (results not shown). Therefore, where the calibration dataset is comprised of a single well, the one-dimensional solution space does not allow a unique estimation of the parameters. However, it does permit the unique estimation of a combination of these parameters, this combination being that provided by the elements of the column of V_1.

The steady-state analysis was repeated with an additional observation well along the *central cross sectio*n. The results are as shown in Table 1B. The S matrix has two non-zero singular values, indicating a solution space dimensionality of 2. Therefore, the null space has only one dimension. The values of K_x and K_{rb} remain highly correlated. However, A_h is uniquely identifiable. Nevertheless, the lower value of the second singular value associated with its estimation results in a high degree of potential contamination of this estimate by noise associated with the calibration dataset. Nevertheless, by taking wells, which are further apart from each other, the uncertainty of estimated A_h can be lowered, because the head difference between these wells is larger compared to potential noise in head measurements. Interestingly, the addition of even more observation wells did not change in any way the results shown in Table 1B. In other words, the dimensionality of the solution space could not be increased through additional head observations. Nevertheless, it allows the estimation of the ratio between K_x and K_{rb} without bias, and of the value of A_h.

The potential gain in parameter identifiability using transient observation data was then explored. The same parameter set was calibrated using a transient head dataset incurred by transience in aquifer heads instigated by river stage variations. This was implemented in the numerical model by varying the heads of the head-dependent boundary that represents the river (Figure 1B). The transience ascribed to this boundary is sinusoidal with an amplitude of 1 m and a period of 2 days. The response of the water table within the aquifer is recorded at intervals of 0.1 days along the *central cross section* at 10 m from the river edge. This provides 10 head observations, equally distributed over a single day, for use as calibration targets. Temporal head differences are used as calibration targets rather than absolute values of heads as it provides some defense against wrong initial conditions (White et al. 2014). Outcomes of the calibration process are shown in Table 1C. In contrast to calibration against a steady-state dataset, the transient dataset provides sufficient information to identify K_{rb}. However, inspection of the matrix V_1 reveals that the level of postcalibration correlation between K_x and A_h is high. Only the value of K_{rb} and the product of K_x with A_h (i.e., K_y) can be estimated with a higher degree of certainty.

In summary, the steady-state calibrations (Table 1A and B) allowed to constrain the value of A_h and the ratio K_x/K_{rb}, provided that at least two head observations at sufficiently different distances from the river were included in the calibration dataset. The transient calibration (Table 1C) supported the estimation of K_{rb}. Therefore, by successively performing a steady-state and a transient calibration, the estimation of the three parameters can be achieved with a higher degree of certainty.

The combined simultaneous effect of these two approaches was tested by calibrating the model using near and far river head values as calibration targets (not the differences) (Table 1D). Two wells, one close to the river edge (10 m) and another sufficiently distant (400 m) were employed as calibration targets to jointly estimate the three parameters. In order to prevent the initial conditions in the aquifer from influencing the estimation process, a spin-up period of 30 days was imposed prior the beginning of the river transience. Outcomes of this transient calibration are presented in Table 1D. The estimation of the three parameters using transient values near and far from the river achieved a dimensionality of the solution space of 3, that is, the

number of parameters requiring estimation. Therefore, the resolution matrix R becomes equal to the identity matrix, indicating that the values of all parameters are individually estimable. Additionally, the matrix V_1 shows that each column is significantly dominated by one parameter.

Following the outcomes of this synthetic analysis, the next section discusses calibration approaches and predictive uncertainty analysis of a real world river-aquifer system located in the glacial valley of the Rhône River (Canton of Valais in Switzerland).

Case Study

The purpose of the case study is the estimation of the values K_x, K_{rb}, and A_h and the analysis of the uncertainty of the prediction of the water table at the airport of Sion (capital of the canton of Valais in Switzerland, Figure 4).

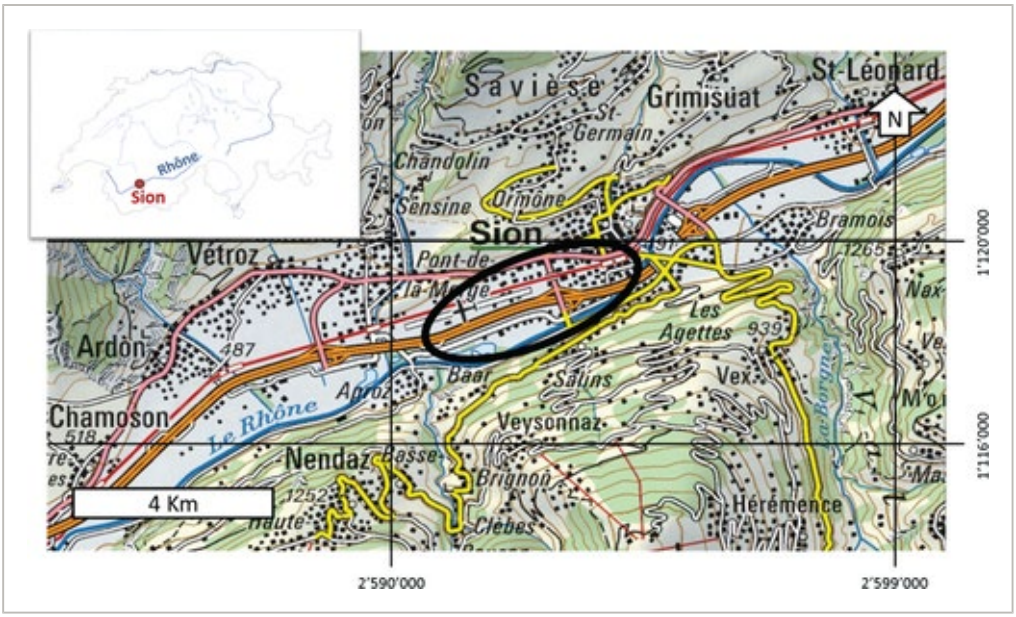

Figure 4

Open in figure viewer | PowerPoint

Situation map of the modeled site. The city of Sion (capital of the canton of Valais, Switzerland), its airport (schematized plane and landing strip) and its communication channels (pink lines: national roads; orange: highways and yellow lines: cantonal roads) crisscrossing the alluvial valley (Swiss national map 1:200000-CN200, reference system CH 1903+/LV95).

Site Description

The site is located in the valley of the Rhône River near the city of Sion (Figure 4). The aquifer consists of alluvial deposits from the Rhône River, which are composed of sandy gravels and silts with an average specific yield S_y of 0.2 (Glenz 2013). The aquifer is unconfined. Hydraulic conductivity values ranging between 10^{-2} and 10^{-4} m/s have been estimated by in situ aquifer tests, analysis of granulometric curves, and by calibration of previous models (Vogel 2003; Rovina+Partner AG 2009; Richon et al. 2010; Glenz 2013).

The nature of alluvial sediments suggests that the alluvial aquifer is likely to be characterized by a certain degree of horizontal anisotropy, with a higher conductivity in the direction of the river corridor, that is, 27° from the east and counterclockwise. The depth of the alluvial aquifer is approximately 40 m (Sartori et al. ; Glenz). It is underlined by lacustrine deposits of clay and silt that can be considered as an

2011 2013
aquitard (Sartori et al. 2011).

Horizontal limits of the model domain are of two types: physical and hydraulic. The lateral physical limits are constituted of geological units of low hydraulic conductivity considered has impervious. Along the aquifer, the model area is limited by equipotential lines, upstream and downstream, which are extracted from the head values of nearby observation wells. Figure 5 shows the 8 observation wells used as calibration targets (w1 to w8) and the location of the prediction.

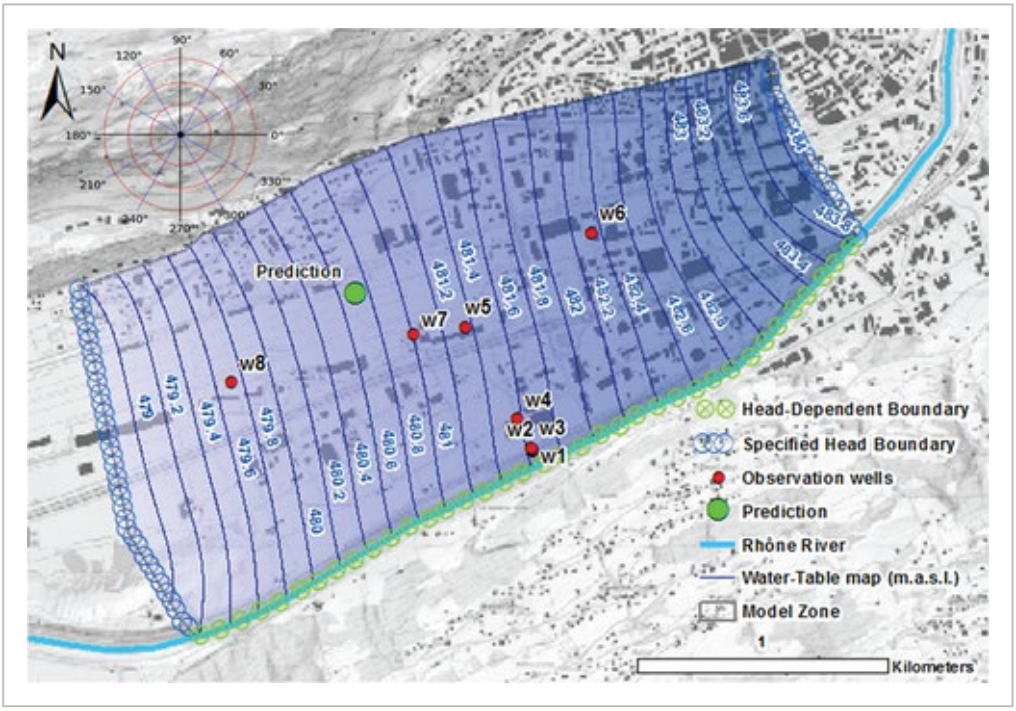

Figure 5

Open in figure viewer | PowerPoint

Model domain (translucent blue area), perimeter boundaries (blue and green circles), observation wells (red dots) and prediction (green dot). The water table map represents a postcalibration head distribution.

Model Calibration and Predictions

Figure 6 presents the estimation of the pre- and post-calibration predictive uncertainties for the approaches a, b, c and d described below.

a) Steady-state calibration (fixed value of the anisotropy). Calibration of the two parameters K_x and K_{rb}. The parameter A_h is assumed to be known and is given a value of 1 defining an isotropic aquifer with respect to its hydraulic conductivity.

b) Steady-state calibration (estimation of the anisotropy). Calibration of the three parameters K_x, K_{rb}, and A_h. As demonstrated in the synthetic analysis, the pre- and postcalibration predictive uncertainty are higher than for the calibration approach (a), due to the added uncertainty on A_h that propagates to the uncertainty of the prediction.

c) Transient calibration constrained by the results of (b) (head difference targets). The three parameters K_x, K_{rb}, and A_h are first estimated using steady-state data (calibration approach (b)). As shown in the synthetic model calibrations, the uncertainty of A_h is reduced. However, the uncertainties in values of

K_x and K_{rb} remain significant after the calibration process, despite the fact that their ratio can be estimated. Their calibrated values and postcalibration uncertainties are then used as initial values and prior uncertainties in the transient calibration, respectively. Then, using only head difference targets, the information content of the near river aquifer response to river transience (w1 in Figure 5) supports a unique estimation of the value of K_{rb} and the already constrained ratio of K_x/K_{rb} allows to provide a unique estimate of K_x. Therefore, the uncertainty of the head prediction resulting from successive steady-state and transient calibrations is significantly lowered.

d) Transient calibration (head value targets). For the case study, an alternative calibration strategy was tested: As opposed to the head difference target, approach (c) the calibration approach here was based on absolute values of heads. This requires a spin-up period of 30 days to generate the initial conditions. The execution time of this calibration strategy is significantly higher than the previous one due the spin-up period. The three parameters K_x, K_{rb}, and A_h are estimated using a transient calibration by fitting the target values of near river and far river heads. The postcalibration predictive uncertainty achieved with this calibration approach is of the same order as that attained through the calibration approach (c).

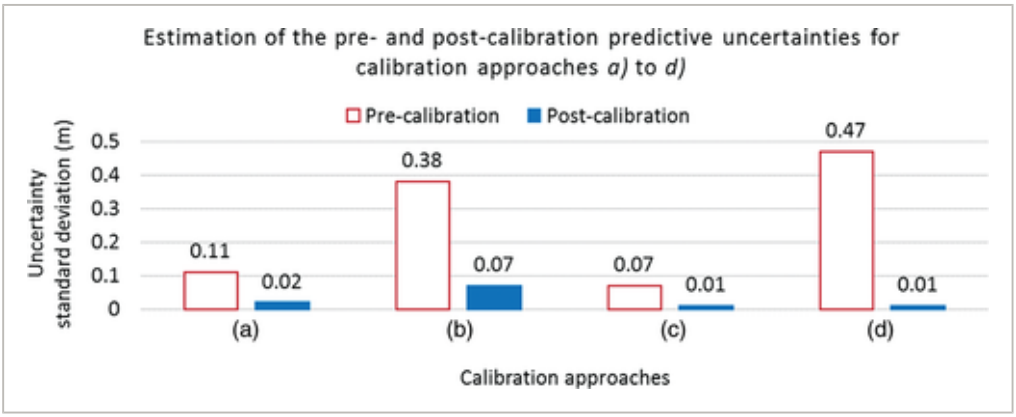

Figure 6

Open in figure viewer | PowerPoint

Graph of the pre- (white rectangles) and postcalibration (blue rectangles) predictive uncertainties calculated for different calibration approaches: steady-state calibrations; steady-state constrained transient calibration (head differences) and transient calibration (head values). See the text for a detailed description of the calibration approaches (a) to (d).

The estimated values of the parameters K_x, K_{rb}, and A_h are, for the approach achieving minimum prediction uncertainty standard deviation (c), 6.6×10^{-4} m/s, 2.3×10^{-7} s^{-1} and 0.27, respectively. Therefore, the hydraulic conductivity parallel to the Rhône River is approximately 3.7 times higher than that perpendicular to the river.

The outcomes of the predictive uncertainty analysis based on the calibration approaches used in the present section are in accordance with the results of the synthetic analysis. In summary, we can observe the underestimation of the predictive uncertainty when the parameter representing the anisotropy of the hydraulic conductivity of the aquifer is omitted from the steady-state calibration process compared to the one for which it is included (see (a) and (b) in Figure 6). Subsequently, the uncertainty of the prediction, computed by the steady-state calibration is further reduced by the information content provided by the transient dataset (see (b) and (c) in Figure 6). The results of (c) are confirmed by the results of the approach (d).

Discussion

We used synthetic and real world numerical models to quantify the implications of falsely assuming isotropic hydraulic properties in an anisotropic environment using modern inversion approaches. The results of this study suggest to include anisotropy as an additional calibration parameter for two key reasons: (1) Our analysis of both the synthetic models and the real world example shows that assuming a value of aquifer anisotropy (including the assumption of isotropic conditions) rather than allowing its adjustment through the calibration process, can lead to significant error in the estimation of key parameters, such as K_x to K_{rb}. These parameters adopt a surrogate role to compensate for the structural error and achieve the better fit. Consequently, their estimations are systematically biased by the structural error. (2) Assuming a value of aquifer anisotropy rather than allowing its adjustment through the calibration process can lead to an underestimation of the uncertainties associated with head predictions in wells that do not comprise the calibration dataset. Given that the uncertainty of the model can no longer be evaluated, its credibility is significantly undermined. One might argue that through the introduction of an additional parameter the inverse problem becomes ill-posed and therefore the number of calibration parameters should not be increased. However, modern calibration codes that include numerical regularization are not troubled when asked to solve an ill-posed inverse problem. In fact, recognition of the ill-posedness of the problem is essential to obtaining a solution to that problem which is of minimized error variance (Doherty 2015).

For the reasons outlined above, history matching based on head targets may lead to a satisfying fit, even if a wrong value for aquifer anisotropy is assumed. This is misleading as the model might be perceived as "well-calibrated" and therefore fit for purpose, despite the underlying structural problems. The value of the post-calibration model-to-measurement misfit depends on the distance between the head targets and the distance from the closest well to the river. Note, however, that in the present synthetic model, structural noise exists only to the extent that horizontal anisotropy is assigned an incorrect value. In real world models additional structural noise (e.g., heterogeneity, vertical anisotropy, etc.) will further contribute to model-to-measurement misfit.

The application of the inverse methods to both steady-state and transient calibration approaches suggests that using steady-state observations can inform the ratio between K_x and K_{rb} as well as the degree of anisotropy. Transient observations provide additional information that allow the unique calibration of these parameters. This, however, is only true for the idealized setup we established here. Further work is required to explore the behavior of other aspects, including aquifer and streambed heterogeneity and more complex forcing functions such as recharge or groundwater abstraction. The calibration tools and the subsequent uncertainty analysis can serve the same purpose as for the idealized systems simulated here and allow to include additional complexities, e.g. the uncertainty of recharge estimations.

Conclusions

Alluvial aquifers typically feature a high degree of anisotropy due to sediment deposition/erosion processes related to fluvial dynamics. Nevertheless, the degree of anisotropy is rarely calibrated. Instead, isotropic conditions or a fixed value of anisotropy are assumed. As a result, the estimated parameters are biased and the uncertainty of predictions are underestimated. This can significantly undermine the credibility of the model predictions. We thus strongly suggest to include anisotropy as an additional calibration parameter, ideally using transient observation of hydraulic heads. Piezometers close to the river are likely to have a higher information content in informating the degree of anisotropy.

This study presented an application of modern estimation and uncertainty analysis in calibration and prediction of environmental models in the context of river-aquifer interactions. The present work supports a broader principle that should be applied to environmental model calibration in general. Where one or more parameters cannot be estimated uniquely, the problem of their non-uniqueness should not be addressed by fixing some and estimating others. This can lead to the adoption of surrogate roles by the estimated parameters and a bias in the estimation of the uncertainties of critical predictions, which may be too low. Risk may therefore be underestimated.

Acknowledgments

This study was funded by the Swiss Confederation and through the project of Third Rhône River Restoration (website: http://www.rhone3.ch). The data used in this paper were also generously provided by the project of Third Rhône River Restoration and thanks to Alexandre Vogel (OCCR3-COTECH). The authors wish to thank Gary Weissmann and the anonymous reviewers for their helpful comments and suggestions. The data and the numerical results used and produced in this paper are available upon request.

References

Citing Literature

Download PDF